International Journal of Scientific Engineering and Applied Science (IJSEAS) – Volume-2, Issue-1, January 2016
ISSN: 2395-3470
www.ijseas.com

MANAGEMENT OF FREQUENCY AND FLUCTUATIONS IN DEMAND GENERATION OF DFIG USING HYBRID SYSTEM

Petla bharani[1] M.Madhusudan Reddy[2]
[1]M.TECH STUDENT, KVSRIT college, Kurnool, AP, INDIA
[2] ASST PROFESSOR,KVSRIT college, Kurnool, AP, INDIA

***Abstract*—This paper presents a control strategy for managing the demand-generation fluctuations using a hybrid energy storage system in a wind-dominated remote area power supply (RAPS) system consisting of a doubly fed induction generator (DFIG), a battery storage system, a supercapacitor, a dump load, and main loads. Operation of a battery storage system is coordinated with a supercapacitor with a view to improving the performance of the battery. In this regard, the battery storage system is connected to the load side of the RAPS system, whereas the supercapacitor is connected to the dc bus of the back-to-back converter of the DFIG. The operation of the hybrid energy storage system is coordinated through the implementation of a power management algorithm, which is developed with a view to reducing the depth of discharge and ripple content of the battery current. In addition, the dump load is connected to the load side of the RAPS system, which utilizes the power in situations that cannot be handled via an energy storage system. In addition, a coordination method has been developed and proposed to coordinate the power flows among all system components with a view to regulating the power flow and thereby ensuring the robust voltage and frequency control on the load side while capturing the maximum power from wind.**

***Index Terms*—Battery storage, coordinated control, doubly fed induction generator (DFIG), maximum power extraction, supercapacitor.**

I. INTRODUCTION

DUE TO THE variable nature of wind (i.e., intermittency), a standalone wind turbine generator alone cannot match the generated power with load demand. In this regard, for a standalone wind farm to be dispatchable similar to other conventional generation units (e.g., diesel generators), the generated power has to be regulated at a desired level. With rapid developments currently taking place on energy storage devices, their application in wind energy systems is seen to provide a promising opportunity to mitigate the issues associated with wind power fluctuations [1]. An energy storage system can be categorized in terms of its role in a remote area power supply (RAPS) system, i.e., either for energy management or for power quality enhancement [2].

An ideal energy storage in a standalone wind energy conversion system should be able to provide both high energy and power capacities to handle situations such as wind gusts and load step changes, which may exist for seconds or minutes or even longer. At present, various types of storage technologies are available to fulfill either power or energy requirements of a RAPS system. Widely advocated energy storage technologies that currently employ in wind farms are batteries, supercapacitors, flywheels, compressed-air energy storage, hydropumped storage, superconducting magnetic energy storage, fuel cells, etc. [3], [4]. Energy storage systems with high energy density levels are usually termed as "long-term storage" as they are able to operate over a long period of time (e.g., minutes to hours). Similarly, energy storage systems with high power density are termed as "short-term storage" as they are capable of handling transients that occur over a short period of time (e.g., seconds to minutes).

Among all energy storage systems, batteries are seen to have one of the highest energy density levels, whereas the supercapacitors seem to have the highest power density. At present, battery storage systems are widely employed in most real-life RAPS applications [5]. To further improve the performance of the battery energy storage systems, a supercapacitor can be incorporated to perform a hybrid operation [6], [7]. In this way, the combined energy storage system is able to satisfy both power and energy requirements of the RAPS system.

Recent studies [8]–[10] in relation to the modeling and control aspects of an energy storage system for a grid connected wind application have received substantial attention. On the contrary, work related to standalone wind energy storage systems has received only little research attention. The applicability of batter storage as the energy storage for a grid connected variable wind generator is described in [9] and [10]. As reported in this literature, the core objective behind the use of the energy storage system (i.e., battery banks) is to mitigate the effect of wind speed fluctuations and thereby to ensure smooth power

.

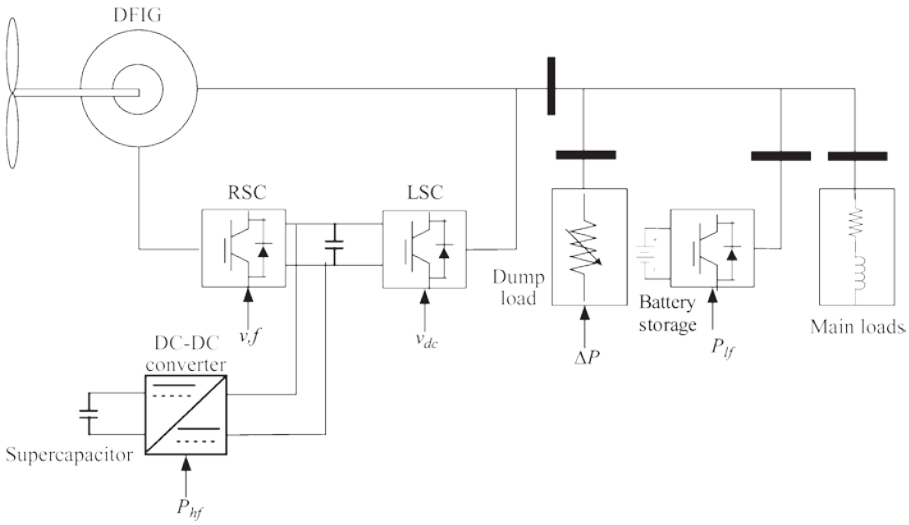

Fig. 1. Hybrid energy storage in a DFIG-based RAPS system.

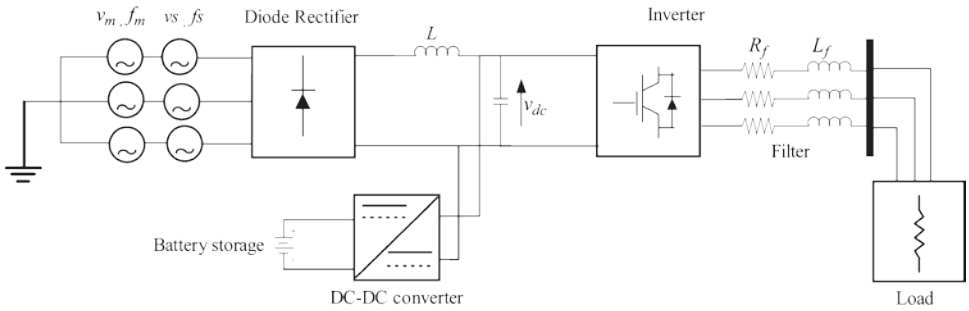

Fig. 2. Schematic of the simplified standalone power supply system.

output from the wind turbine generator. A hybrid energy storage system, including both battery system and supercapacitor, for a grid connected variable wind turbine generator is discussed in [6]. The application of a hybrid energy storage system for grid connected and standalone wind energy applications is given in [6] and [11], respectively. This literature particularly focuses on the performance of the hybrid energy storage system rather than considering the system-level investigations.

The RAPS system considered in this paper is shown in Fig. 1 consisting of a wind turbine generator; a hybrid energy storage system, namely, battery energy storage and supercapacitor; a dump load; and main loads. In this regard, individual controllers for the system components have been developed, and their operations are coordinated with a view to regulating the load-side voltage and frequency and to extracting maximum power from wind. In addition, a power management algorithm is implemented between two energy storage devices (i.e., battery storage and supercapacitor) with a view to ensuring safer operation of the battery storage system by avoiding higher depth of discharges (DODs). The suitability of the propped RAPS system is investigated under changing wind and fluctuating load conditions.

This paper is organized as follows. Section II illustrates the importance of having integrated an energy storage system for renewable energy (i.e., wind) application. The significance of hybrid energy storage for a wind energy application is also illustrated in this section. Section III discusses the proposed control coordination methodology employed among the components in the RAPS system. The detailed information of the proposed power management algorithm adopted to the battery energy storage system and supercapacitor is described in Section IV. The individual control strategies developed for each RAPS system component [e.g., doubly fed induction generator (DFIG) and battery energy storage] are given in Section V. The simulated results of the proposed RAPS system are presented in Section VI. Conclusions are given in Section VII.

II. Benefits of Integrating Energy Storage for RAPS System

Two examinations that are based on two different circuits shown in Figs. 2 and 6 are used to illustrate the benefits of having integrated: 1) battery energy storage; and 2) hybrid energy storage for wind energy application, respectively.

The arrangement shown in Fig. 2 can be used to investigate the benefits of having energy storage for a standalone wind system. To represent the intermittency associated with the wind turbine power output, a variable power supply that consists of a steady component v_m of 230 V at a fundamental frequency f_m of 50 Hz and a variable supply at a frequency f_s of 120 Hz[1] with a voltage source of magnitude v_s of 50 V is used.

[1]As reported by the authors in their earlier paper [12], DFIG operation can introduce low-order harmonics caused by the slip and multiple armature reaction. Moreover, as reported in [13], DFIG can introduce interharmonics such as 80 and 120 Hz.

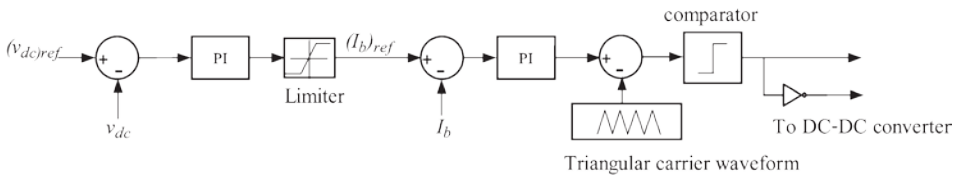

Fig. 3. Controller for the energy storage system.

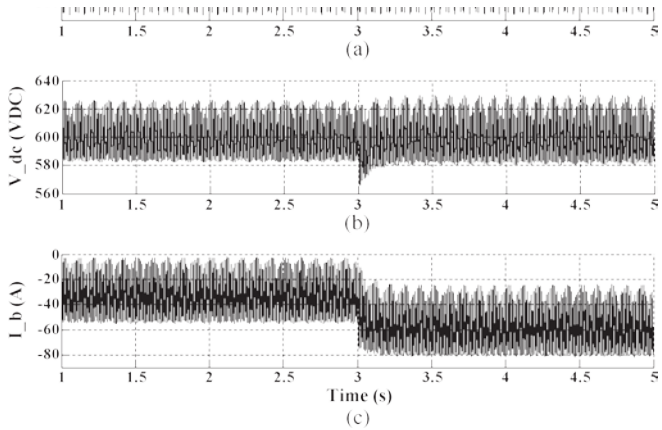

Fig. 4. RAPS system performance with the battery storage system: (a) supply voltage, (b) dc link voltage, and (c) battery current.

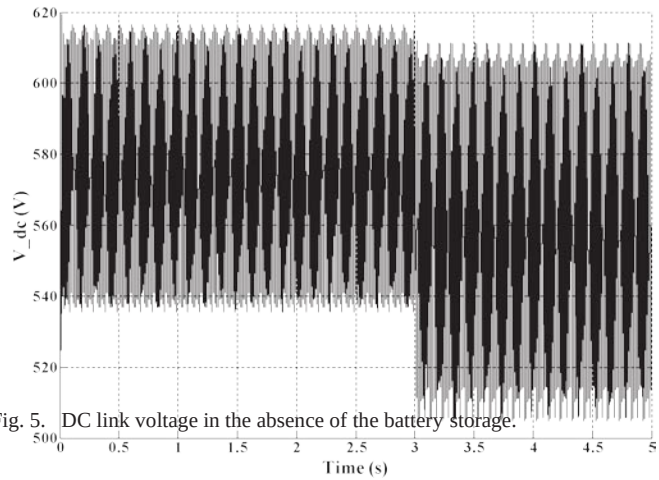

Fig. 5. DC link voltage in the absence of the battery storage.

As shown in Fig. 2, a battery system is selected to represent the energy storage system, which is incorporated into the dc bus of the wind energy system. The main objective of the battery storage system is to regulate dc bus voltage v_{dc}. In this regard, a bidirectional boost converter is used to interface the battery storage system to the dc bus. The conditions under which the battery storage system is operated can be explained by (1). Any power imbalance associated with the RAPS system shown in Fig. 2 can lead to a dc bus voltage variation. Hence, the dc bus voltage variation is used as the input signal of the controller, as shown in Fig. 3, for the battery storage system

$$\text{battery status} = \begin{cases} \text{charging mode}, & \Delta v_{dc} > 0 \\ \text{discharging mode}, & \Delta v_{dc} < 0 \\ \text{idling mode}, & \Delta v_{dc} = 0. \end{cases} \quad (1)$$

The suitability of the energy storage system, which helps in regulating the dc link voltage, is observed under fluctuating wind and load conditions. Initially, the load is set at 25 kW, and after $t = 3$ s, the load demand is increased to 40 kW. The supply-side voltage, which is used to simulate the power output of the wind turbine generator, is shown in Fig. 4(a). The simulated behavior of the dc bus and load-side voltage with and without the energy storage system are shown in Figs. 4(b) and 5, respectively. The corresponding battery storage current is shown in Fig. 4(c). It is shown that the dc link voltage is regulated within ±5% of its rated value (i.e., 600 V) in the presence of the battery storage system. In contrast, the variation of dc link voltage without the battery storage system is seen to vary within +5% and −15% of its rated value. This simulation exercise clearly indicates the benefits of the energy storage system for a standalone wind application. However, it can be noted that the current of battery energy storage is fluctuating rapidly. This may adversely affect the life span of the battery storage system. Therefore, it is vital to hybridize the operation of the battery storage system with a supercapacitor that could relive the fluctuating effects in operation of the battery storage system.

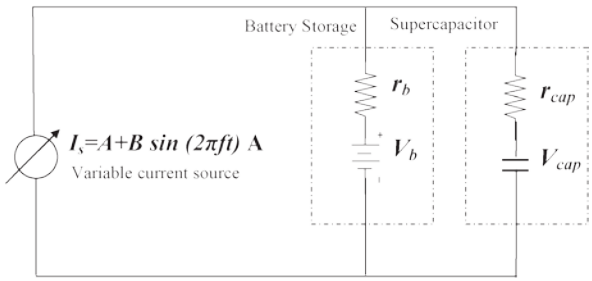

Fig. 6. Simplified model of a power system with hybrid energy storage.

A simple arrangement[2] shown in Fig. 6 is used to demonstrate the significance of integrating hybrid energy storage into a standalone wind power application where the fluctuating current source represents the variable wind power output, which consists of two components. The main steady component corresponds to dc current with a magnitude of $A = 50$ A and a ripple component of $B = 7.5$ A at $f = 20$ Hz that is superimposed on the main component to simulate the fluctuating power component of the wind turbine generator. The battery storage system is represented by the series resistor r_b with a constant dc voltage source v_b of 25 V. The supercapacitor is represented

[2] i.e., without employing any control.

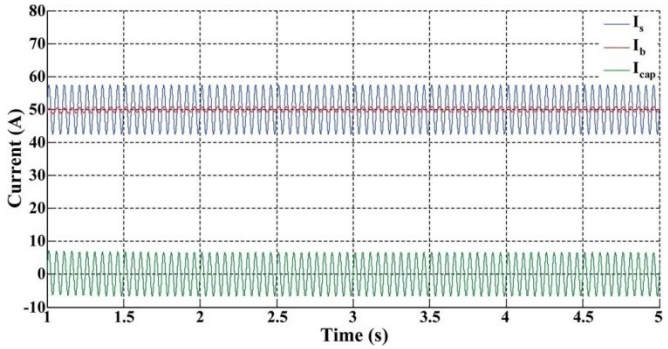

Fig. 7. Current sharing between battery storage and supercapacitor.

by a capacitor of which the voltage is v_{cap}, connected in series with resistor r_{cap}.

The simulated behavior of the system is shown in Fig. 7. It is shown that the fluctuating component of the current is absorbed by the supercapacitor, whereas the battery storage system absorbs the steady component of 50 A. The fluctuation of the battery current is limited to ±1 A, thus ensuring safe operation of the battery storage system. The above example demonstrates the benefits of having integrated a supercapacitor with battery energy storage for effectively mitigating the ripple content of the battery current.

III. Proposed Coordinated Control Approach for Hybrid Energy Storage-Based RAPS System

The decision-making process associated with the control coordination algorithm of the wind–battery–supercapacitor-based RAPS system is shown in Fig. 8. During overgeneration conditions where the power output from the wind turbine generator P_w is greater than the load demand P_L, the hybrid energy storage P_b (i.e., battery storage and supercapacitor) absorbs the excess power $(P_w - P_L)$ and is shared between the battery storage system and supercapacitor according to the power management algorithm presented in Section IV.[3] If the capacity of the hybrid energy storage system reaches the maximum limit or $(P_b)_{max}$, the dump load needs to absorb the excess power. However, if the dump load power P_d reaches its maximum rating $(P_d)_{max}$, the pitch angle control has to be activated in order to reduce the power output of the wind turbine generator. During undergeneration situations where the power output of the wind turbine generator is less than the load demand, i.e., $(P_w - P_L) < 0$, it is assumed that the hybrid energy storage P_b is able to supply the required power deficit $(P_L - P_w)$. During emergency situations such as no power output from wind turbine generator due to wind speed being below cut-in level or above cut-out level, a load shedding scheme can be implemented, which is not given an emphasis in this paper. Moreover, the proposed control coordination concept has been realized by developing the control strategies for each component of the RAPS system.

[3]According to the proposed power management algorithm, the supercapacitor should be able to absorb the ripple or high-frequency power component of demand-generation mismatch leaving the steady component for the battery storage system.

It is assumed that the entire reactive power requirement of the RAPS system Q_L is satisfied using DFIG, i.e., Q_{DFIG}. More information regarding the reactive power generation through the DFIG is illustrated in Section V-A. However, it is to be noted that, for the case where a higher value of reactive power is required, a capacitor bank can be installed.

IV. Proposed Power Management Algorithm for Hybrid Energy Storage System

Depending on the objectives to be achieved (e.g., minimization of the demand-generation mismatch and ensuring safe operation of the energy storage systems), a power management algorithm can be designed and implemented for the hybrid energy storage system. The proposed power management algorithm is designed in such a way that the supercapacitor should be able to absorb the ripple or high-frequency power component of demand-generation mismatch leaving the steady component for the battery storage system. As indicated in Section III, the power management algorithm is implemented encompassing the battery storage and supercapacitor with a view to achieving the following objectives:

1) to help maintain the power balance of the RAPS system;
2) to operate the wind turbine generator based on the maximum power point tracking (MPPT) algorithm;
3) to improve the performance of the battery storage system by reducing ripple current and high rate of DOD.

The first objective is achieved by generating the input signal for the controllers of the hybrid energy storage system using the demand-generation mismatch $(P_w - P_L)$ of the RAPS system. To realize the second objective, the wind power output P_w of the demand-generation mismatch is estimated using the optimal wind power $(P_w)_{opt}$ given by (2)–(4). By controlling the power flow into/out of the battery storage system and supercapacitor, it is possible to impose an appropriate torque on the wind turbine generator to extract the maximum power from wind. In this way, maximum power tracking algorithm is embedded with the power management scheme to extract the maximum available power from wind

$$(P_w)_{opt} = k_{opt}[(\omega_r)_{opt}]^3 \tag{2}$$

$$k_{opt} = \frac{1}{2}(C_p)_{opt}\rho A\left(\frac{R}{\lambda_{opt}}\right)^3 \tag{3}$$

$$\lambda_{opt} = \frac{(\omega_r)_{opt} R}{v} \tag{4}$$

where $(C_p)_{opt}$ is the optimum power coefficient of the turbine, A is the area swept by the rotor blades, v is the wind speed, ρ is the air density, R is the radius of the blade, λ_{opt} is the optimum tip-speed ratio, β is the pitch angle, and $(P_w)_{opt}$ is the optimal wind power output.

Under heavy DOD levels, the battery storage attains quick charge regulation, as shown in Fig. 9. Therefore, the third objective is related to managing the DOD levels of the battery storage system, which is achieved by separating the demand-generation mismatch into two frequency components through a high-pass filter $\tau s/1+\tau s$, as shown in Fig. 10. The

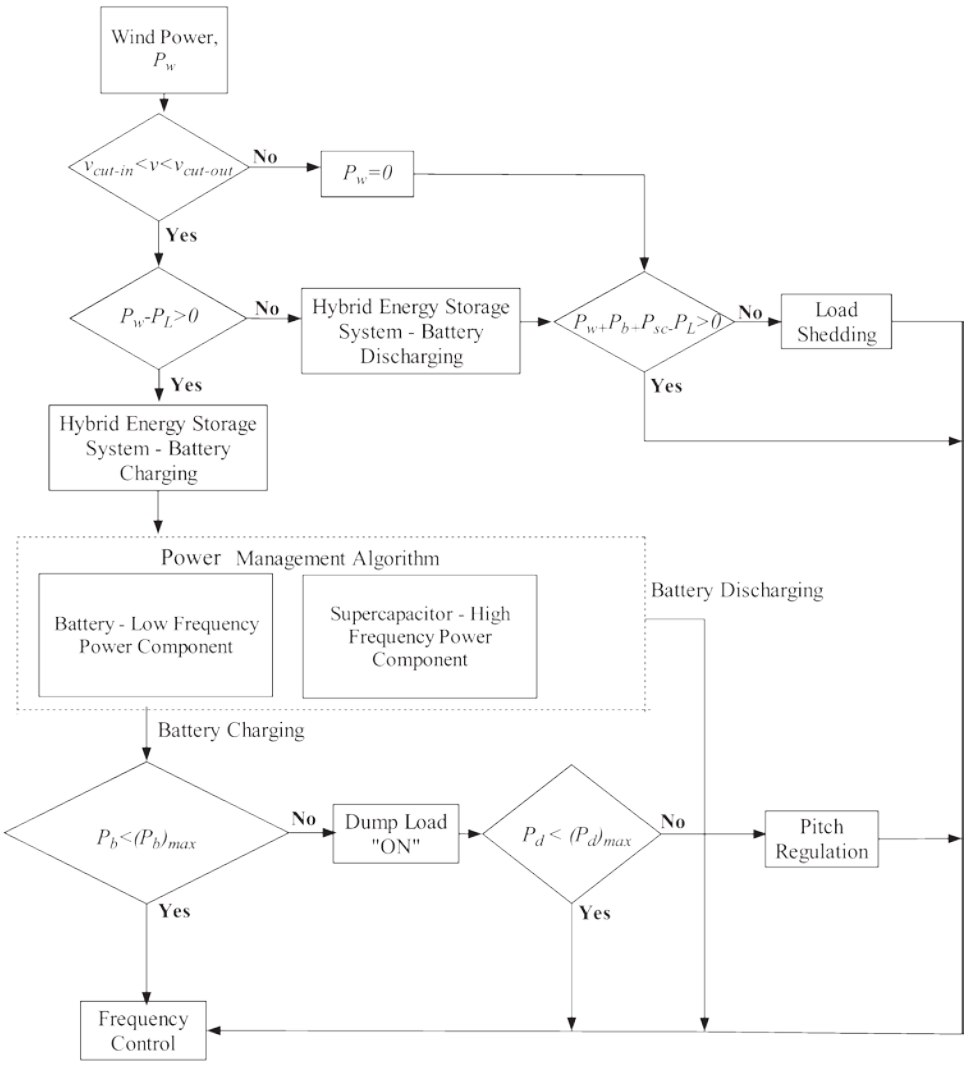

Fig. 8. Control coordination of a wind–battery–supercapacitor-based hybrid RAPS system.

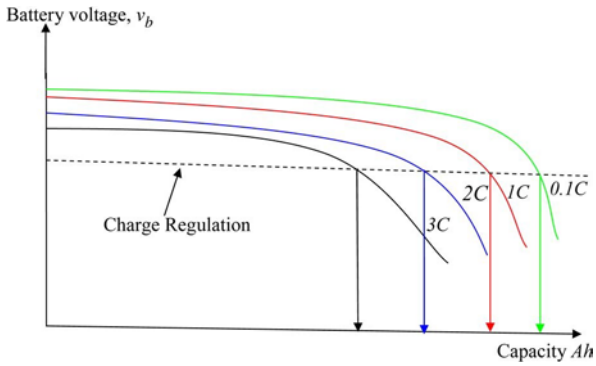

Fig. 9. Battery voltage under different discharge rates. (*C* denotes the discharge rate of the battery storage system.)

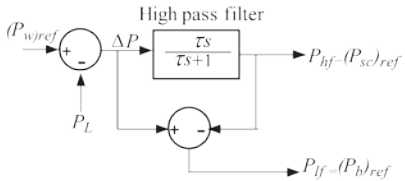

Fig. 10. Estimation of reference power for battery storage and supercapacitor.

demand-generation mismatch is explained by two frequency regions, which can be given by (5). The high-frequency power component of the demand-generation mismatch P_{hf} is used to estimate the reference current of the supercapacitor $(i_C)_{ref}$. Contrarily, the low-frequency power component of the demand-generation mismatch P_{lf} is used to generate the reference current of the battery storage $(i_b)_{ref}$. The operating frequency range of each type of energy storage systems is diagrammatically shown in Fig. 11[4]

$$\Delta P_{wL} = P_{hf} + P_{lf} \tag{5}$$

where P_{hf} is the high-frequency component of the demand-generation mismatch, and P_{lf} is the low-frequency component of the demand-generation mismatch.

Considering the operating frequency range as the criterion, two different models of a supercapacitor can be depicted, as

[4] f_c represents the cutoff frequency of the filter circuit. Typically, f_c is 0.5 Hz [6].

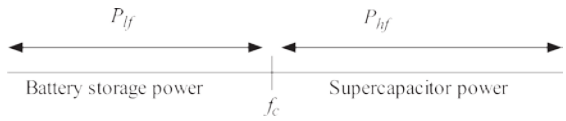

Fig. 11. Operating frequency ranges of the energy storage systems: Supercapacitor and battery storage system.

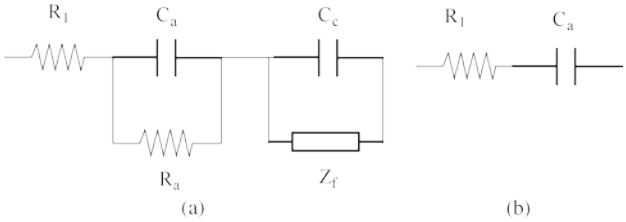

Fig. 12. Equivalent circuits of supercapacitor. (a) High-frequency model. (b) Low-frequency model.

shown in Fig. 12. The first model indicated in Fig. 12(a)[5] is known as detailed model, which includes the nonlinear Faraday capacitance. The low-frequency domain model, which can be used under power system operating frequency range[6] presented in Fig. 12(b) is employed in the current work.

In real-life applications, the operation of a supercapacitor needs to satisfy the conditions given in (6)–(8). The first condition given by (6) emphasizes the safe operating voltage of a supercapacitor, which is usually indicated in the manufacturer data sheet. The second condition given by (7) indicates the maximum possible peak current of a supercapacitor. The third condition presented in (8) defines the maximum allowable power from the supercapacitor during its operation

$$(v_{sc})_{min} < v_{sc} < (v_{sc})_{max} \tag{6}$$

$$(I_c)_{pk} = \frac{0.5 C_{sup} v_{sc}}{C^{sup}(ESR_{dc}) + 1} \tag{7}$$

$$(P_{sc})_{max} = \pm\, C_{sup} v_{sc} \left| \frac{dv_{sc}}{dt} \right|_{max} \tag{8}$$

where C_{sup} is the capacitance value of the supercapacitor; $(v_{sc})_{max}$, $(v_{sc})_{min}$ are maximum and minimum operating voltages of supercapacitor, respectively; ESR_{dc} is the equivalent series resistor of the supercapacitor; $(P_{sc})_{max}$ is the maximum power rating of the capacitor, and $|dv_{sc}/dt|_{max}$ is the maximum rate of change of voltage across the supercapacitor.

The size estimation of the battery energy storage and supercapacitor is extremely design specific for a given site or an application. However, in the present case, the value of the capacitance of the supercapacitor is estimated considering the worst case scenario where it is able to supply energy subjected to the wind energy inverter constraints over a certain time period t, as given by (9) and (10). Furthermore, the size of the battery storage system is estimated using the condition given in (11) as follows:

$$E_{sc} = (s_{max}(P_{DFIG})_{rated})\, t \tag{9}$$

$$C_{sup} = \frac{2E_{sc}}{((v_{sc})_{max})^2 - ((v_{sc})_{min})^2} \tag{10}$$

$$\mu \times i_{rated} \times \frac{t}{60} = (\text{Ah rating}) \times k^r \tag{11}$$

where μ is the fraction of the rated current of the load demand, i_{rated} is the rated current corresponding to the load demand, t is the time duration over which the battery provides power to the system, and k^r is a fraction that defines the average discharge/charge current of the battery storage.

V. Design of Controllers for Individual System Components

As shown in Fig. 1, the battery storage is connected to the load side using an inverter, whereas the supercapacitor is interfaced to the dc bus of the back-to-back converter system by means of a bidirectional buck boost converter. The operation of the entire RAPS system is designed according to the proposed coordinated control approach given in Fig. 8. The control strategies associated with the battery storage system, supercapacitor, and dump load are illustrated in the following sections.

A. DFIG Control

The rotor-side converter (RSC) and line-side converter (LSC) are modeled as current-controlled voltage source inverters in which the field-oriented vector control schemes are employed to develop the respective control schemes. The control objectives that are related to RSC and LSC can be listed as follows:

1) RSC: voltage and frequency control on the stator side;
2) LSC: dc bus voltage control of the back-to-back converter system and it provides reactive power if necessary for loads.

The voltage controller of the DFIG is developed using a reactive-power-based control approach. In this regard, the total stator reactive power output Q_s of the DFIG can be given as

$$Q_s = \frac{3}{2}\left[-\frac{v_s^2}{\omega L_s} + v_s \frac{L_m}{L_s} i_{dr} \right]. \tag{12}$$

The rotor d-axis current i_{dr} consists of two components, i.e., magnetizing current i_{drmag}, which is used to compensate the no-load reactive power of the DFIG, and i_{drgen}, which is utilized to satisfy the reactive power requirements of the loads. The corresponding reactive power components of these two currents, namely, Q_{mag} and Q_{gen}, are given by (13) and (14), respectively,

$$Q_{mag} = \frac{3}{2}\left[-\frac{v_s^2}{\omega L_s} + v_s \frac{L_m}{L_s} i_{drmag} \right] \tag{13}$$

$$Q_{gen} = \frac{3}{2} \frac{L_m}{L_s} v_s\, i_{drgen}. \tag{14}$$

[5] R_1 represents the equivalent series resistance, C_a is the anode dielectric capacitance, R_a is equivalent parallel resistance of dielectric materials, C_F is the cathode Faraday capacitance, and Z_f is the Faraday impedance, which includes the resistance of charge movement that is not a pure resistance [11].

[6] In this case, the power system operating frequency is 50 Hz.

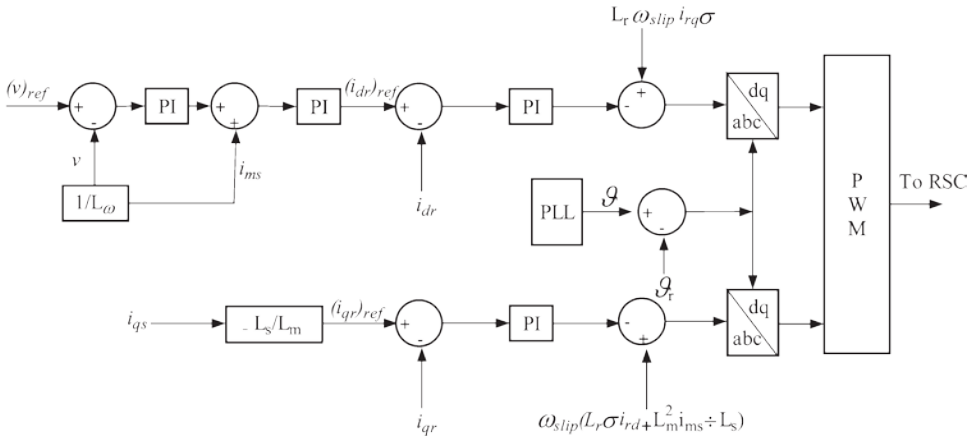

Fig. 13. RSC control scheme of DFIG.

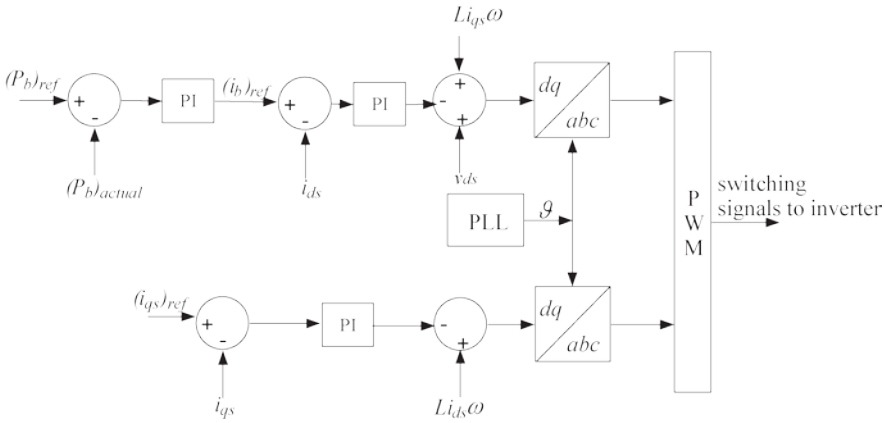

Fig. 14. Inverter control used for battery storage system.

The no-load reactive power can be compensated by imposing the condition given by (15). In addition, the reference current of i_{drgen} can be established by considering the voltage error, which is compensated through a PI controller, as shown in (16). Therefore, the reference d-axis component of the current that is used to satisfy the magnitude of the stator voltage can be given in (17) as follows:

$$i_{\text{drmag}} = \frac{v_s}{\omega L^m} \tag{15}$$

$$(i_{\text{drgen}})_{\text{ref}} = (k_p + k_i)\,((v_s)_{\text{ref}} - v_s) \tag{16}$$

$$(i_{dr})_{\text{ref}} = (i_{\text{drgen}})_{\text{ref}} + i_{\text{drmag}} \tag{17}$$

where k_p and k_i are proportional and integral gains of the PI controller, respectively.

The indirect stator flux orientation scheme for the machine is ensured by setting the q-axis component of the stator flux to zero. This condition can be achieved by setting i_{qr} as given in (18) and is regarded as a criterion that needs to be followed in order to maintain the frequency

$$i_{qr} = -\frac{L_s}{L_m} i_{qs}. \tag{18}$$

Therefore, the q-axis component of the rotor current given in (18) is considered as the reference q-axis component of the rotor current, which is used to achieve frequency regulation. In addition, a virtual phase-locked loop (PLL) is used to define the reference frequency for the entire control scheme of the RSC, as shown in Fig. 13.

The voltage orientation scheme (i.e., making $v_{qs} = 0$ in the stator voltage) is employed for control purposes of the LSC. The reactive power can be controlled using the q-axis component of the stator current, and the d-axis component is used to regulate the dc link voltage. However, the reactive power provision through the LSC is made to zero by setting the reference q-axis component of the stator current to zero. The PI controllers associated with RSC and LSC are tuned using the internal model control principle, as discussed in [14].

B. Battery Storage Controller

As stated in Section IV, the battery storage is used to meet the steady component of the demand-generation mismatch, thus avoiding higher depths of discharging. As shown in Fig. 1, an inverter is used to interface the battery storage system with the RAPS system. The inverter control[7] associated with the battery storage is developed by following the power management algorithm and depicted in Fig. 14. The reference current of the battery $(i_b)_{\text{ref}}$[8] is generated considering the low-frequency

[7]Refer to Appendix B for more information.

[8]$(i_b)_{\text{ref}}$ is used to represent the $(i_{\text{ds}})_{\text{ref}}$ in Fig. 14.

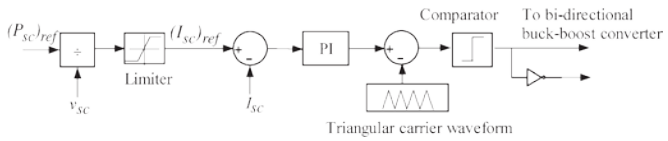

Fig. 15. Control strategy for the supercapacitor in hybrid energy storage.

component of the demand-generation mismatch P_{lf},[9] as given in (19). The inverter is operated at unity power factor by setting $(i_{qs})_{ref}$ equal to zero. The PI controllers associated with control schemes shown in Fig. 14 are tuned using the Ziegler–Nichols method, as given in [15]

$$(i_b)_{ref} = (P_{lf} - P_b)(k_p + k_i/s) \quad (19)$$

where P_b is the actual battery power, and k_p and k_i are the proportional and integral gains of the PI controller, respectively.

C. Supercapacitor Controller

The low-frequency model of a supercapacitor consisting of a capacitor and a resistor, which can be used under power system operating frequency range,[10] is employed in the current work. As shown in Fig. 1, the supercapacitor is connected to the dc bus of the back-to-back converter using a bidirectional buck–boost converter system. The high-frequency component of the demand-generation mismatch P_{hf} [11] is met by the supercapacitor where the corresponding reference current $(i_{sc})_{ref}$ is estimated using (20). The adopted control strategy for the supercapacitor is illustrated in Fig. 15

$$(i_{sc})_{ref} = \frac{P_{hf}}{v_{sc}}. \quad (20)$$

D. Dump Load Controller

Dump load is represented by a series of resistors that are connected across switches. The resistors are used to operate at zero crossings of the voltage to ensure minimum impact on the quality of system voltage. As stated in Section III, the operation of dump load is enabled when the battery storage reaches its maximum capacity. Therefore, the condition under which the dump load operation is enabled is given by (21). It is to be noted that the contribution of the supercapacitor power is not considered in the process of estimating the dump load power considering its performance in a short-term window and a high-frequency domain. The simplified schematic of the dump load controller is shown in Fig. 16

$$P_d = \begin{cases} P_d, & (P_w) + (P_b)_{max} - P_L > 0 \\ 0, & \text{otherwise} \end{cases} \quad (21)$$

where P_w is the power output of the DFIG, and $(P_b)_{max}$ is the maximum capacity of the battery storage.

[9] $P_{lf} = (P_b)_{ref}$, where $(P_b)_{ref}$ is the reference battery power shown in Fig. 14.

[10] In this case, the power system operating frequency is 50 Hz.

[11] $P_{hf} = (P_{sc})_{ref}$, where $(P_{sc})_{ref}$ is the reference supercapacitor power shown in Fig. 15.

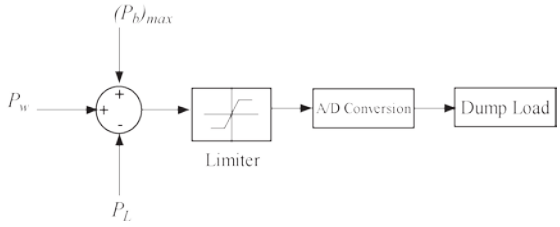

Fig. 16. Dump load control strategy.

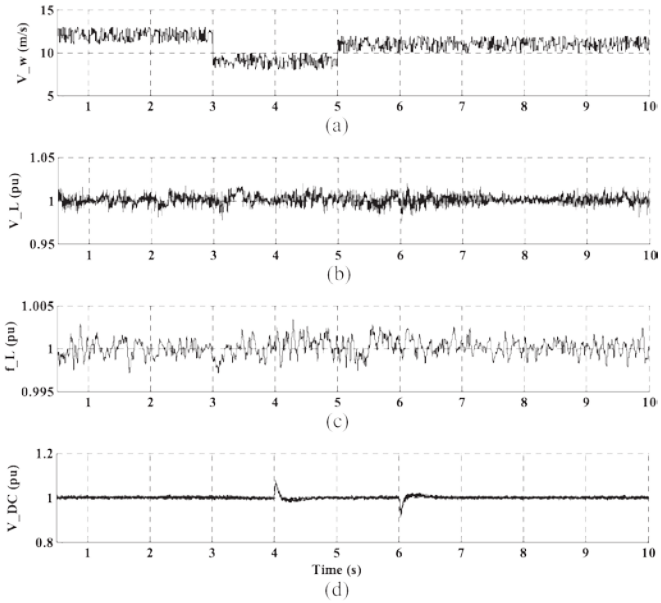

Fig. 17. Response of the DFIG-based RAPS system during variable wind and load conditions: (a) wind speed, (b) voltage on the load side, (c) frequency on the load side, and (d) dc link voltage.

VI. Performance Evaluation of the Hybrid Energy Storage in a DFIG-Based RAPS System

The system response of the DFIG-based RAPS system is shown in Fig. 17. Fig. 18 illustrates the power sharing between different system components. The wind condition under which the system has been simulated is shown in Fig. 17(a). It is shown that the wind velocity is set initially at 12 m/s. At t = 3 s, the wind velocity drops to 9 m/s, and it increases to 11 m/s at t = 5 s. As shown in Fig. 18(d), initial load demand is set at 0.425 p.u., and then it is increased to a value of 0.7 p.u. at t = 4 s and the added additional load (i.e., 0.275 p.u.) is disconnected from the system at t = 6 s. The voltage on the load side is shown in Fig. 17(b), which is not seen to be affected by the wind speed or resistive load step changes. The load voltage of the system stays within ±2% of its rated value throughout the operation. The operating frequency of the RAPS system is shown in Fig. 17(c). As anticipated, the operating frequency is closely regulated at its rated value of 1.0 p.u. and is not seen to be influenced by the wind speed or load step changes. Furthermore, it can be seen that the frequency of the system is maintained within ±0.2% of its rated value. The dc link voltage of the DFIG is depicted in Fig. 17(d), which is well regulated at its rated value throughout the operation except during load step changes. However, the highest dc link voltage variations are seen to occur at t = 4 s

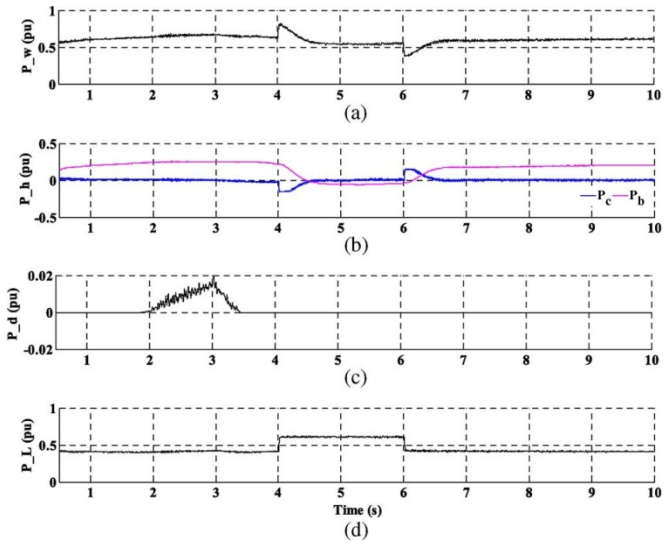

Fig. 18. Power sharing of the DFIG-based wind–hybrid energy storage RAPS system during variable wind and load conditions: (a) wind power, (b) hybrid energy storage power (i.e., battery power P_b and supercapacitor power P_{sc}), (c) dump load power, and (d) load demand.

and $t = 6$ s, which correspond to the load step changes, as evident from Fig. 17(d). It can be noted that the supercapacitor quickly changes its direction of power flow, as evident from Fig. 18(b), which causes the fluctuations in the dc link voltage. However, even during such transient conditions, the dc link voltage variation is limited to within ±10% of its rated value.

The DFIG power output is shown in Fig. 18(a). For simulation purposes, initially, the slip of the wind turbine is set to $s = -0.1$, which corresponds to super synchronous mode of operation. According to the wind turbine characteristics, the corresponding maximum power output of the wind generator is 0.73 p.u. at the speed of 1.2 p.u. for a wind speed of 11 m/s. As shown in Fig. 18(a), the power output of the DFIG is seen to rise to a value of 0.69 p.u. at $t = 3$ s, and the corresponding load demand is at 0.425 p.u. This situation simulates an over-generation condition where the excess power is shared between the battery storage system and supercapacitor, as evident from Fig. 18(b). It is shown that the supercapacitor responds to the fast-varying power variations, whereas the battery absorbs the slow-varying power variations of the demand-generation mismatch. In addition, the supercapacitor quickly responds to load step changes that occur at $t = 4$ s and $t = 6$ s avoiding high rates of DOD of the battery storage system. Furthermore, the battery storage system reaches its full capacity at $t = 2$ s leading to the operation of dump load, which absorbs the additional power, as evident from Fig. 18(c). The battery storage system operates in its charging mode until load step addition, which occurs at $t = 4$ s leading to a change of its mode of operation from charging to discharging. However, the rate of discharge is reduced after the load step reduction that occurs at $t = 6$ s. The MPPT behavior of the DFIG is shown in Fig. 19. It is shown that DFIG closely follows the MPPT curve except during the transient conditions that occur at $t = 4$ s and $t = 6$ s.

The battery current for the case with no supercapacitor is shown in Fig. 20. The battery current consists of a high-frequency fluctuating component, and it exhibits steep DOD

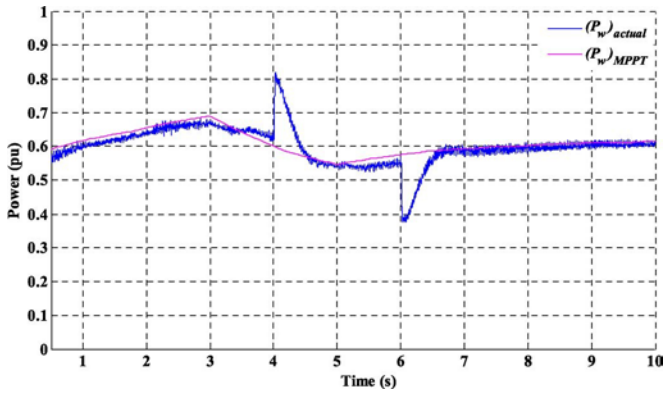

Fig. 19. MPPT tracking capability of the DFIG in a RAPS system with energy storage integrated.

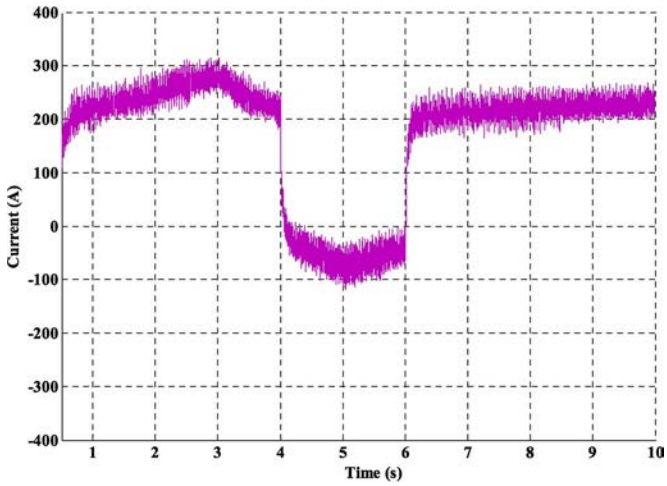

Fig. 20. Battery current for the case with no supercapacitor of the DFIG based RAPS system with hybrid energy storage integrated.

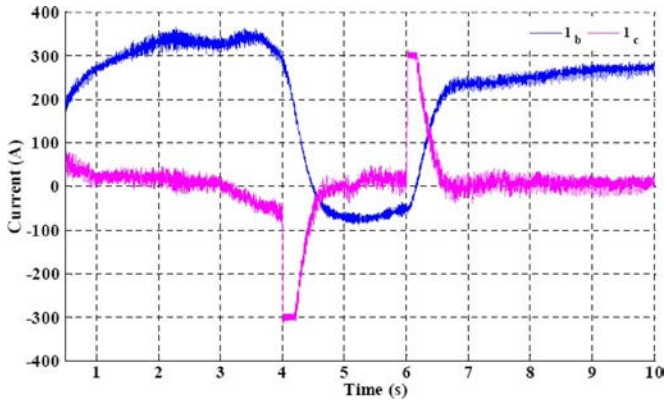

Fig. 21. Currents of the hybrid energy storage: battery current i_b and supercapacitor current i_c of the DFIG-based RAPS system.

during load step changes. The current levels of the hybrid energy storage with the supercapacitor are shown in Fig. 21. It is shown that the battery storage system has less fluctuations in its current with low DOD rate at the time of load step changes compared with the case where it operates alone without a supercapacitor.

The supercapacitor current consists mostly of high-frequency component and is seen to quickly respond to the transients.

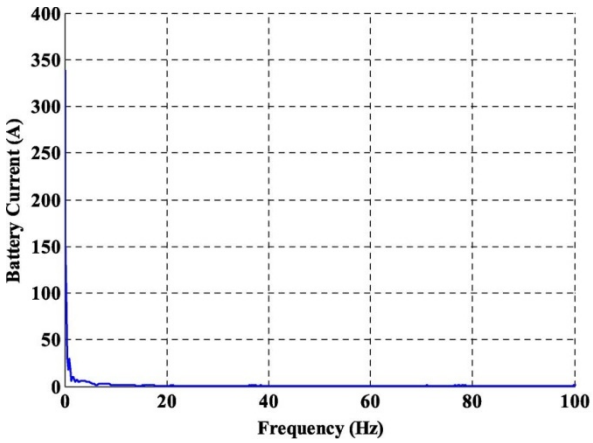

Fig. 22. Frequency spectrum of the battery storage system of hybrid energy storage.

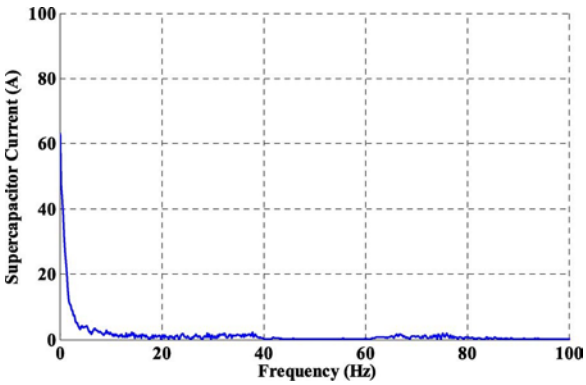

Fig. 23. Frequency spectrum of the supercapacitor in hybrid energy.

However, the safety feature integrated with the controller of the supercapacitor has limited its current to 300 A.[12]

The frequency spectra of the battery current and the supercapacitor current are given in Figs. 22 and 23, respectively. The battery current is shown to be free from ripples or high-frequency component, whereas the supercapacitor current consists of considerable amount of high frequencies,[13] which ensures the safe operation of the battery storage.

VII. Conclusion

This paper has addressed the benefits of integrating a supercapacitor to a battery storage system in a wind-based hybrid RAPS system. In this regard, a power management algorithm has been established between the battery storage system and supercapacitor to operate both energy storage systems in a designated manner. In addition, to coordinate the power flow between the RAPS system components, a control coordination strategy was developed and implemented by incorporating the aforementioned power management algorithm. Furthermore, the following conclusions can be drawn.

1) The proposed RAPS system is able to regulate the voltage and frequency on the ac side within tight limits.
2) The algorithm to satisfy demand-generation mismatch has been implemented using the proposed power management algorithm where the demand-generation mismatch of the RAPS systems was split in the two frequency operating regions using a high-pass filter. The high-frequency power component was managed through the supercapacitor while leaving the low-frequency power component for the battery storage system.
3) The maximum power extraction through the DFIG has been achieved by coordinating the operation of hybrid energy storage system by implementing the maximum power extraction algorithm.
4) The reduction of the rate of DODs has been achieved by operating the supercapacitor to respond the high-frequency power component associated with the demand-generation mismatch, thus avoiding high rate of DOD on the battery energy storage system.

TABLE I
Parameters Associated With RAPS System

Rated power output (P_{DFIG})	750 kW
Stator resistance (R_s)	0.00706 pu
stator Leakage inductance (L_{ls})	0.171 pu
Rotor resistance (R_r)	0.005 pu
Rotor leakage inductance (L_{lr})	0.156 pu
Magnetising inductance (L_m)	2.2 Vs
Inertia constant (H)	2.04 S
Number of pole pairs (P)	3
Filter inductance at LSC (L_f)	0.3 pu
Filter resistance at LSC (R_f)	0.3/100 pu
DC bus voltage (v_{dc})	750 V
Stator voltage (v_s)	400 V
Operating frequency (f_s)	50 Hz
Rating of battery storage system (P_b)	420 kWh
Capacitance of Supercapacitor (C)	20 F
Allowable SOC of the battery system (SoC)	40%-80%
Rated dump load power ($(P_d)_{max}$)	200 kW

Appendix A

The parameters associated with the RAPS system are shown in Table I.

Appendix B
Battery Inverter Control for DFIG-Based RAPS System

The control algorithm associated with the inner current control loop of the battery inverter system given in Section V-B can be described as follows:

$$v_{ds1} = v_{ds} - v_{ds}^{*} + L_f \omega i_{qs} \quad \text{(B.1)}$$

$$v_{qs} - L_f \omega i_{ds} \quad \text{(B.2)}$$

$$v_{ds}^{*} = R_f i_{ds} + L_f \frac{di_{ds}}{dt} \quad \text{(B.3)}$$

$$v_{qs}^{*} = R_f i_{qs} + L_f \frac{di_{qs}}{dt} \quad \text{(B.4)}$$

by $0.5C_{sup}V/C_{sup}(ESR_{dc}) + 1$, where ESR_{dc} is the equivalent series resistor [16].

[13]In this paper, the battery storage is used to respond the power fluctuations below 0.5 Hz, whereas the high-frequency power variations are managed through the supercapacitor.

where v_a, v_b, and v_c are the voltages on the load side; i_a, i_b, and i_c are the currents through the filter circuit; L_f and R_f are filter inductance and resistance, respectively; v_{a1}, v_{b1}, and v_{c1} are the voltages at the inverter output; v_{ds} and v_{qs} are the d- and q-axis components of the load-side ac voltage, respectively; i_{ds} and i_{qs} are the d- and q-axis components of the inverter current, respectively; and v_{ds1} and v_{qs1} are the d- and q-axis components of the inverter output voltage, respectively.

The d- and q-axis reference currents of the battery inverter can be generated by defining the reference active and reactive power components, as given in (B.5) and (B.6), respectively,

$$(i_{ds})_{\text{ref}} = ((P_b)_{\text{ref}} - P_b)\,(K_{pdb} + K_{idb}/s) \quad \text{(B.5)}$$

$$(i_{qs})_{\text{ref}} = ((Q_b)_{\text{ref}} - Q_b)\,(K_{pqb} + K_{iqb}/s) \quad \text{(B.6)}$$

where $(P_b)_{\text{ref}}$ and $(Q_b)_{\text{ref}}$ are the reference active and reactive power outputs of the battery inverter, and K_{pdb}, K_{pqb} and K_{idb}, K_{iqb} are the proportional and integral gains of the battery inverter controller.

Appendix C
Estimation of Supercapacitor Size

The supercapacitor is used to supply $s_{\max}$ times the rated capacity of the DFIG power, i.e., P_{DFIG}. The safe operating voltage limits associated with the supercapacitor are selected to be as follows:

$$250\ \text{V} < v_{\text{sc}} < 500\ \text{V}. \quad \text{(C.1)}$$

Assuming that, in the worst case scenario, the supercapacitor is able to provide the maximum slip power of DFIG $s_{\max}P_{\text{DFIG}}$ for time $t = 10$ s, the capacitance value of the supercapacitor can be calculated as follows:

$$C = \frac{s_{\max}(P_{\text{DFIG}})_{\text{rated}}t}{((v_{\text{sc}})_{\max})^2 - ((v_{\text{sc}})_{\min})^2} \quad \text{(C.2)}$$

$$C = \frac{0.3 \times 750 \times 1000 \times 10 \times 2}{500^2 - 200^2} \approx 20\ \text{F}. \quad \text{(C.3)}$$

References

[1] M.-S. Lu, C.-L. Chang, W.-J. Lee, and L. Wang, "Combining the wind power generation system with energy storage equipment," *IEEE Trans. Ind. Appl.*, vol. 45, no. 6, pp. 2019–2115, Nov./Dec. 2009.
[2] Q. Li, S. S. Choi, Y. Yuan, and D. L. Yao, "On the determination of battery energy storage capacity and short-term power dispatch of a wind farm," *IEEE Trans. Sustainable Energy*, vol. 2, no. 2, pp. 148–158, Apr. 2011.
[3] P. F. Ribeiro, B. K. Johnson, M. L. Crow, A. Arsoy, and Y. Liu, "Energy storage systems for advanced power applications," *Proc. IEEE*, vol. 89, no. 12, pp. 1744–1756, Dec. 2001.
[4] M. Beaudin, H. Zareipour, A. Schellenberglabe, and W. Rosehart, "Energy storage for mitigating the variability of renewable electricity sources: An updated review," *Energy Sustainable Develop.*, vol. 14, no. 4, pp. 302–314, Dec. 2010.
[5] T. Patrick and Moseley, "Energy storage in remote area power supply (RAPS) systems," *J. Power Sources*, vol. 155, no. 1, pp. 83–87, Apr. 2006.
[6] W. Li, G. Joos, and J. Belanger, "Real-time simulation of a wind turbine generator coupled with a battery supercapacitor energy storage system," *IEEE Trans. Ind. Electron.*, vol. 57, no. 4, pp. 1137–1145, Apr. 2010.
[7] P. Thounthong, S. Rael, and B. Davat, "Control strategy of fuel cell and supercapacitors association for a distributed generation system," *IEEE Trans. Ind. Electron.*, vol. 54, no. 6, pp. 3225–3233, Dec. 2007.
[8] L. Qu and W. Qiao, "Constant power control of DFIG wind turbines with supercapacitor energy storage," *IEEE Trans. Ind. Appl.*, vol. 47, no. 1, pp. 359–367, Jan./Feb. 2011.
[9] S. Teleke, M. E. Baran, A. Q. Huang, S. Bhattacharya, and L. Anderson, "Control strategies for battery energy storage for wind farm dispatching," *IEEE Trans. Energy Convers.*, vol. 24, no. 3, pp. 725–732, Sep. 2009.
[10] A. Abedini and H. Nikkhajoei, "Dynamic model and control of a wind-turbine generator with energy storage," *IET Renew. Power Gen.*, vol. 5, no. 1, pp. 67–78, Jan. 2011.
[11] W. Li and G. Joos, "Dynamic model and control of a wind-turbine generator with energy storage," in *IEEE PESC*, Rhodes, Greece, Jun. 2008, pp. 1762–1768.
[12] N. Mendis, K. Muttaqi, and S. Perera, "Voltage quality behaviour of a wind turbine based remote area power system," in *Proc. IEEE ICIT*, Gippsland, Australia, Feb. 10–13, 2008, pp. 1–6.
[13] S. T. Tentzerakis and S. A. Papathanassiou, "The harmonics of the slip energy recovery drive," *IEEE Power Eng. Rev.*, vol. 21, no. 4, pp. 55–57, Apr. 10–13, 2001.
[14] L. Harnefors and H. P Nee, "Model-based current control of AC machines using the internal model control method," *IEEE Trans. Ind. Appl.*, vol. 34, no. 1, pp. 133–141, Jan./Feb. 1998.
[15] J. C. Basilio and S. R. Matos, "Design of PI and PID controllers with transient performance specification," *IEEE Trans. Educ.*, vol. 45, no. 4, pp. 364–370, Nov. 2002.
[16] [Online]. Available: http:www.maxwell.com/products